





Article

Targeted Mass Spectrometry Reveals Interferon-Dependent Eicosanoid and Fatty Acid Alterations in Chronic Myeloid Leukaemia

Hannah C. Scott^{1,2,*}, Simeon D. Draganov^{1,2}, Zhanru Yu^{1,2}, Benedikt M. Kessler^{1,2,†} 
and Adán Pinto-Fernández^{1,2,*} 

¹ Chinese Academy of Medical Sciences Oxford Institute, Nuffield Department of Medicine, University of Oxford, Oxford OX3 7BN, UK; simeon.draganov@ndm.ox.ac.uk (S.D.D.); zhanru.yu@ndm.ox.ac.uk (Z.Y.); benedikt.kessler@ndm.ox.ac.uk (B.M.K.)

² Target Discovery Institute, Centre for Medicines Discovery, Nuffield Department of Medicine, University of Oxford, Oxford OX3 7FZ, UK

* Correspondence: hannah.scott@ndm.ox.ac.uk (H.C.S.); adan.pintofernandez@ndm.ox.ac.uk (A.P.-F.)

† These authors have contributed equally to this work.

Abstract: Bioactive lipids are involved in cellular signalling events with links to human disease. Many of these are involved in inflammation under normal and pathological conditions. Despite being attractive molecules from a pharmacological point of view, the detection and quantification of lipids has been a major challenge. Here, we have optimised a liquid chromatography–dynamic multiple reaction monitoring–targeted mass spectrometry (LC-dMRM-MS) approach to profile eicosanoids and fatty acids in biological samples. In particular, by applying this analytic workflow to study a cellular model of chronic myeloid leukaemia (CML), we found that the levels of intra- and extracellular 2-Arachidonoylglycerol (2-AG), intracellular Arachidonic Acid (AA), extracellular Prostaglandin F_{2α} (PGF_{2α}), extracellular 5-Hydroxyeicosatetraenoic acid (5-HETE), extracellular Palmitic acid (PA, C16:0) and extracellular Stearic acid (SA, C18:0), were altered in response to immunomodulation by type I interferon (IFN-I), a currently approved treatment for CML. Our observations indicate changes in eicosanoid and fatty acid metabolism, with potential relevance in the context of cancer inflammation and CML.

Keywords: bioactive lipids; eicosanoids; fatty acids; mass spectrometry; lipidomics; innate immunity; type I interferon response; chronic myeloid leukaemia; cancer inflammation; cancer metabolism



Citation: Scott, H.C.; Draganov, S.D.; Yu, Z.; Kessler, B.M.; Pinto-Fernández, A. Targeted Mass Spectrometry Reveals Interferon-Dependent Eicosanoid and Fatty Acid Alterations in Chronic Myeloid Leukaemia. *Int. J. Mol. Sci.* **2023**, *24*, 15513. <https://doi.org/10.3390/ijms242115513>

Academic Editor: Juan Antonio Giménez-Bastida

Received: 19 September 2023
Revised: 17 October 2023
Accepted: 18 October 2023
Published: 24 October 2023



Copyright: © 2023 by the authors. Licensee MDPI, Basel, Switzerland. This article is an open access article distributed under the terms and conditions of the Creative Commons Attribution (CC BY) license (<https://creativecommons.org/licenses/by/4.0/>).

1. Introduction

Bioactive lipids regulate cellular functions and contribute to tissue homeostasis and pathology [1]. Four families of bioactive lipids are involved in inflammation and immune regulation: eicosanoids, specialised pro-resolving mediators, lysoglycerophospholipids/sphingolipids and endocannabinoids, which are generated from ω -3 or ω -6 polyunsaturated fatty acids (PUFAs). Eicosanoids are key elements in inflammation, and have been linked with diseases, such as viral infections, neurodegenerative disorders [2], rheumatoid arthritis [3], atherosclerosis [4,5], acute coronary syndrome [6], cancer [7,8], systemic lupus erythematosus [9], multiple sclerosis [10], liver injury [11], celiac disease [12], diabetes [13], cystic fibrosis [14], renovascular disease [15], asthma [16] and muscle dysfunction [17]. In addition, fatty acids, the common components of complex lipids, often act as immunomodulatory factors [18,19].

In general, lipids are challenging molecules to characterise due to the limited analytical capacity to identify, quantify and annotate them in biological samples, which has been an impediment to the advancement of discovering molecular mechanisms of disease, biomarker discovery and drug development. Mass spectrometry (MS) approaches,

predominantly in combination with liquid chromatography (LC), are widely used for the analysis of biomolecules [20–23], including eicosanoids [24,25]. More recently, LC has been coupled with dynamic multiple reaction monitoring (dMRM) workflows for the targeted detection of specific subsets of eicosanoids [26,27], and high-resolution (MRMHR) methods to generate a library of high-resolution fragmentation spectra [28] have been developed. In addition, eicosanoid profiling by LC-MS has previously been performed on human plasma [29], clinical samples [30] and mouse models of pathophysiological states [31]. However, such analyses remain challenging due to limitations in the accurate assignment and detection of endogenous species [32,33]. One reason is a lack of thoroughness in optimising truly representative sample matrix variations, instead of using “surrogate matrices” (such as BSA in a sample buffer, which would be a matrix approximation) and applying more efficient extraction methodologies adapted to specific lipid subsets within specific sample types (e.g., cell and cell supernatant samples).

In this study, an intracellular and extracellular analysis (the media in which the respective cells are cultured) of eicosanoids and fatty acids was performed using a tailored extraction and dMRM method to maximise the sensitivity of the detection of endogenous species. Since bioactive lipids such as eicosanoids have important roles in inflammation and cancer, we performed a proof-of-concept experiment to study the effect of the pro-inflammatory cytokine interferon α 2 (IFN α -2b, hereafter IFN-I) on HAP1 cells. HAP1 cells were derived from a chronic myeloid leukaemia (CML) patient and have been extensively used in different translational studies [34–36]. IFN-I is a cytokine secreted by most cells in response to viral infection, and has known immunostimulatory and anticancer properties [37]; specifically, the IFN-I subtype IFN α 2 has been approved, alone and in combination with tyrosine kinase inhibitors (TKIs), for the treatment of CML [38].

Here, due to the optimisation of a novel LC-dMRM-MS targeted method suitable for the analysis of a selection of eicosanoids and fatty acids in cells and supernatants, we were able to uncover changes in the lipidome of CML samples induced by a clinically relevant treatment, IFN-I. These lipids were selected for their known roles in inflammation and immune signalling, especially within the context of cancer and CML. For the subset of eicosanoids, we endeavoured to include representatives of as many different types as possible, such as the 5-HETE family, Leukotrienes and Prostaglandins. The selection process was also dependent on standard availability and compatibility with LC/MS analytical conditions such as chromatographic separation and ionisation efficiency.

Of particular interest, we found that IFN-I affected intra- and extracellular concentrations of 2-Arachidonoylglycerol (2-AG), the intracellular concentration of Arachidonic Acid (AA) and the extracellular concentrations of Prostaglandin F $_{2\alpha}$ (PGF $_{2\alpha}$), 5-Hydroxyeicosatetraenoic acid (5-HETE), Palmitic acid (PA, C16:0) and Stearic acid (SA, C18:0), suggesting a role of these lipids in the inflammatory state of CML tumours that has not yet been described.

2. Results

A representative group of eicosanoids and fatty acids (Figure 1a) was selected based on their inflammatory roles and potential regulation by IFN-I. We focused on improving the identification and separation of lipid standards (chromatographic separation), their ionisation (source parameters) and their quantitation by developing and implementing a dMRM method. We also applied this method to biological samples, where we optimised the amount of starting material, the lipid extraction method, and determined the specific matrix effects upon each lipid in two sample types (cells and cell supernatant), as shown in Figure 1b.

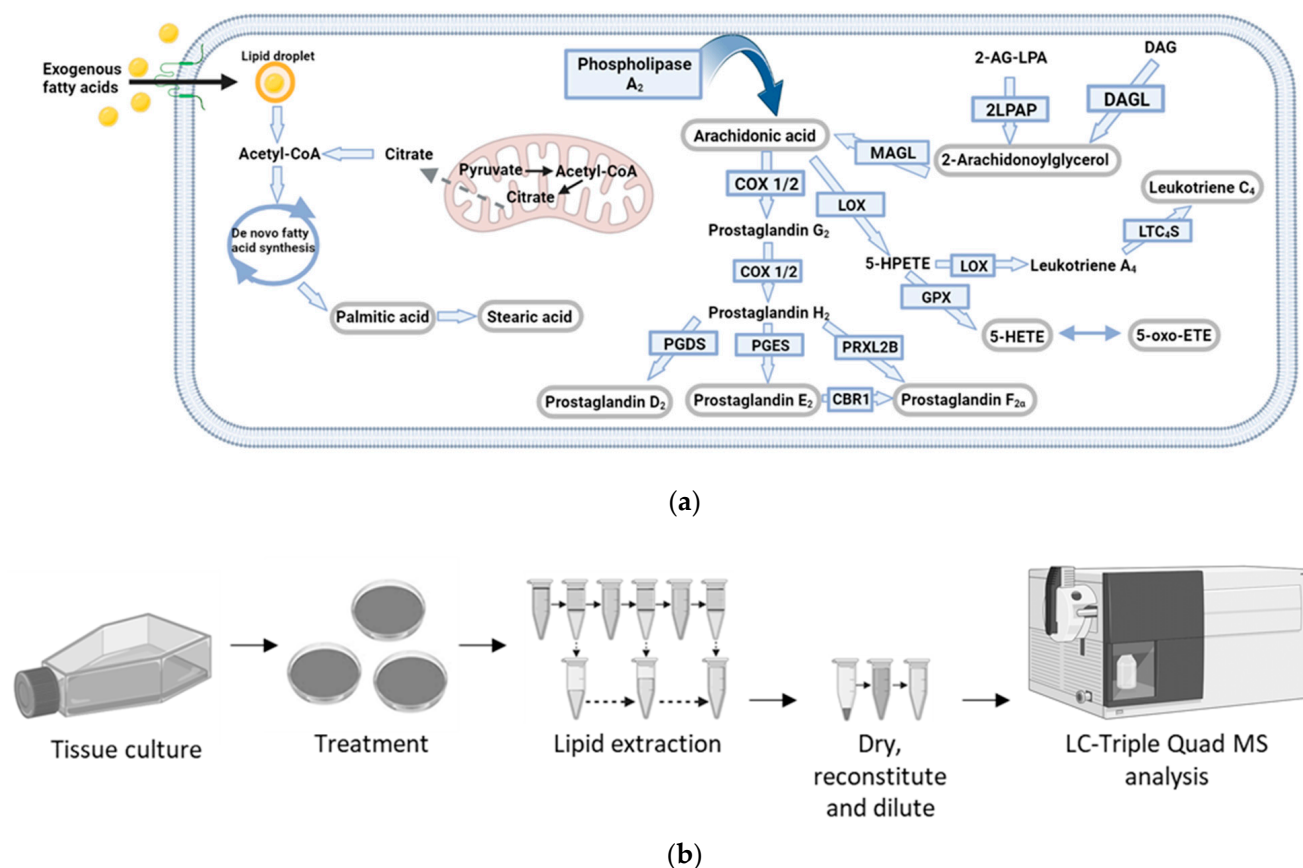


Figure 1. Eicosanoid pathway and methodology workflow. (a) Metabolic pathways of selected bioactive lipids. Converting enzymes are in boxes and the lipids in this study are circled in grey. De novo lipogenesis leading to fatty acid synthesis, which results in the elongation of fatty acids, produces Palmitic acid and Stearic acid. Exogenous fatty acid uptake is carried out via transmembrane transporters. (b) Optimised experimental workflow for the analysis of eicosanoids and fatty acids was conducted using ultra-high-performance liquid chromatography–dMRM–MS (UPLC–dMRM–MS). Cells were cultured in IMDM media containing 10% foetal bovine serum (FBS) and grown until 60–70% confluent. Cells were then treated with 1000 U/mL of IFN α -2b for 36 h, reaching ~80% confluence. The surrounding media (the cell supernatant) was collected from the plates and cells were lysed. Lipid extraction from cells and cell supernatants was performed with Methanol/Methyl tert-butyl ether/chloroform (MeOH/MTBE/CHCl₃) and acetonitrile (ACN), respectively. Lipid extracts were subsequently dried and reconstituted in 50% (*v/v*) MeOH (in H₂O) prior to LC–MS analysis.

2.1. Liquid Chromatography–Dynamic Multiple Reaction Monitoring–Mass Spectrometry (LC–dMRM–MS) Method Optimisation for Bioactive Lipid Standards

The analysis of lipid standards (Table 1) was first performed in MS¹ mode to detect the corresponding precursor ions. Following tandem mass spectrometry (MS/MS; MS²), an extracted ion chromatogram of the most intense fragment ion was used for lipid assignment. The MS² spectra were then compared to either acquired or predicted MS² spectra in the Human Metabolome Database (HMDB) for confirmation of identity by using one to three fragment ions as a reference, as shown in Figure S1a (Supplementary Materials). Once discovered, the retention time was then used to assign the retention time window in the dMRM acquisition parameters.

Table 1. Optimised transitions for LC-dMRM-MS. Lipid names, dMRM parameters and lower limits of quantification (LLOQ) are listed for all eicosanoid and fatty acid standards analysed. The CE used for the precursor-to-product ion transitions are indicated in electron volts (eV).

Lipid	Formula	Molecular Weight (g/mol)	Retention Time (min)	Precursor Ion (<i>m/z</i>)	Precursor Ion Type	Product ion <i>m/z</i> (Qualifiers)	Product CE (Voltage)	Product Ion <i>m/z</i> (Quantifier)	Quantifier CE (Voltage)	LLOQ (on Column Concentration)
5-oxo-EETE	C ₂₀ H ₃₀ O ₃	318.22	2.5	319.2	[M+H] ⁺	91.1 43.1 55.1	56 48 68	189	12	500 amol/L
Aracidonic acid	C ₂₀ H ₃₂ O ₂	304.24	3.8	305.25	[M+H] ⁺	58.3 92.1 65.2	28 44 80	91.1	32	20 fmol/L
2-Arachidonoylglycerol	C ₂₃ H ₃₈ O ₄	378.30	7.4	379.3	[M+H] ⁺	91.1 67.2 79.1	72 64 68	287.2	16	100 amol/L
Palmitic acid	C ₁₆ H ₃₂ O ₂	256.43	8.3	257.25	[M+H] ⁺	43.2 57.2 55.2	36 16 48	41.2	68	5 fmol/L
Prostaglandin D ₂ /E ₂	C ₂₀ H ₃₂ O ₅	350.22	8.3	391.2	[M+K] ⁺	105 63.1 271	24 44 4	312.8	0	5 fmol/L
Stearic acid	C ₁₈ H ₃₆ O ₂	248.27	10.3	285.28	[M+H] ⁺	57.3 120.9 41.2	20 8 72	43.3	36	100 zmol/L
Prostaglandin F _{2α}	C ₂₀ H ₃₄ O ₅	354.24	10.3	377.2	[M+Na] ⁺	57 43.3 342.2	48 64 12	360.3	4	5 amol/L
5-HETE	C ₂₀ H ₃₂ O ₃	320.24	11.8	338.30	[M+NH ₄] ⁺ / [M+H ₂ O] ⁺	55.5 41.3 203.3	56 76 20	43.2	52	500 amol/L
Leukotriene C ₄	C ₃₀ H ₄₇ N ₃ O ₉ S	625.3	14.9	664.26	[M+K] ⁺	57.2 629.5 125	72 24 44	496.3	36	500 amol/L

Implementing dMRM increases the ion of interest's response by removal of interfering signals (noise) and acquiring data on specific product ions only when the corresponding precursor ion is present. dMRM also improves dwell times during data acquisition by applying a retention time window that restricts when data are obtained for specific transitions, resulting in superior signal-to-noise (S/N) ratios. Non-overlapping ion transmissions also optimises dwell time and therefore sensitivity. dMRM transitions of lipid standards (Table 1) were identified using the Agilent MRM optimiser software (v. B.07.00), which applies a collisional energy (CE) ramp and suggests transitions based on the abundance and the mass-to-charge ratio (*m/z*) values. Manual checking of these transitions was performed, as the ion implied to have the highest abundance by the software (the quantitation ion, the "quant ion") did not always align with the ion with the actual greatest response. By this method, we have identified up to four dMRM transitions that can be used as quant and qualifier ions ("qual ions") (Table 1 and Figure S1b,c). The "quant ion" is used for quantification, and the other three ions ("qual ions") are used to corroborate identification. Analysis of lipids in the presence of ammonium acetate (which is our mobile phase modifier) can create ammonium adduct ions of lipids. In our methodology, an example of this phenomenon is the precursor ion of 5-HETE, which was an ammonium adduct with a *m/z* of 338.3. Structures of all lipid standards analysed and the corresponding proposed quant ion structures are shown in Figure S1d.

The chromatographic separation of lipids reduces the complexity of biological samples and decreases matrix effects. The chromatogram, in Figure S1e, displays the dMRM transitions for an equimolar ratio of all the lipids profiled. On the x-axis is the elution time (counts vs. acquisition time, also known as the retention time), and on the y-axis is the response (counts, AUC = area under curve). Not all responses are the same for all the lipids, even when at the same on-column concentration, as lipids are ionised at different efficiencies. Interestingly, it was not possible to chromatographically separate the regio-isomers species PGD₂ and PGE₂ reliably or sufficiently enough to determine their individual concentra-

tions with this particular methodology. The results reported here are to be interpreted as the concentration of one, the other or both those metabolites combined. Otherwise, our method has sufficiently adequate separation, preventing overlapping MRMs, which results in longer scan times for each MRM, increasing the points per peak for each lipid. In the case of the co-eluting compounds, for example SA and PGF_{2α}, compound-specific precursor and product ions allow for their accurate identification.

We observed that the retention time for certain lipids could have a slight variation at different column loadings; therefore, the dMRM retention time window in the analysis method (used to trigger data acquisition for the respective transition at that particular time) was set wider for those lipids. In addition, peak shape can also change at different column loadings, with shoulders or tails on some peaks; therefore, we have included these in our analysis. For some lipids, lower on-column concentrations appeared to result in jagged, not smooth, peaks; therefore, it was necessary to add smoothing during data processing. To further improve the ionisation efficiency of lipids, all MS parameters were adjusted to an optimal value (Table 2). For example, we found that a source gas temperature of 80 °C was optimal for the identification of intact lipids by MS², due to a lower degree of in-source fragmentation, allowing for the identification of fairly intact lipids. However, for dMRM analysis, the most optimal precursor-to-product ion responses were obtained at a source gas temperature of 280 °C. Once the optimal MS parameters were determined, we subsequently validated the robustness and reproducibility of our optimised method by intraday variation analysis, whereby lipid standards were combined and analysed in technical triplicate at two concentrations, 0.3 and 3 pmol on-column, respectively (Figure 2). The coefficient of variation (CV) was calculated between the mean of technical replicates at both concentrations. The observed CVs for all the lipids are lower than 20%, and lower than 5% for most lipids (six out of nine lipid standards), highlighting the repeatability of this method.

Table 2. Chromatography and mass spectrometry parameters. This table represents the instrumentation settings used in the analysis method and the parameters applied. Settings are selected for the most favourable separation and ionisation of eicosanoids and fatty acids.

Chromatography Setting	Parameter
Mobile phase composition	A = 2% IPA, 5mM Ammonium Acetate B = 100% IPA, 5mM Ammonium Acetate
Mobile phase flow rate (mL/min)	0.21
C18 column temperature (°C)	40
Source setting	Parameter
Gas temperature (°C)	280
Gas flow (L/min)	14
Nebulizer (psi)	20
Sheath gas temperature (°C)	250
Sheath gas flow (L/min)	11
Capillary: positive and negative polarity (V)	3000
Nozzle: positive and negative polarity (V)	1500
iFunnel setting	Parameter
High Pressure RF: positive polarity (V)	150
Low pressure RF: positive polarity (V)	60

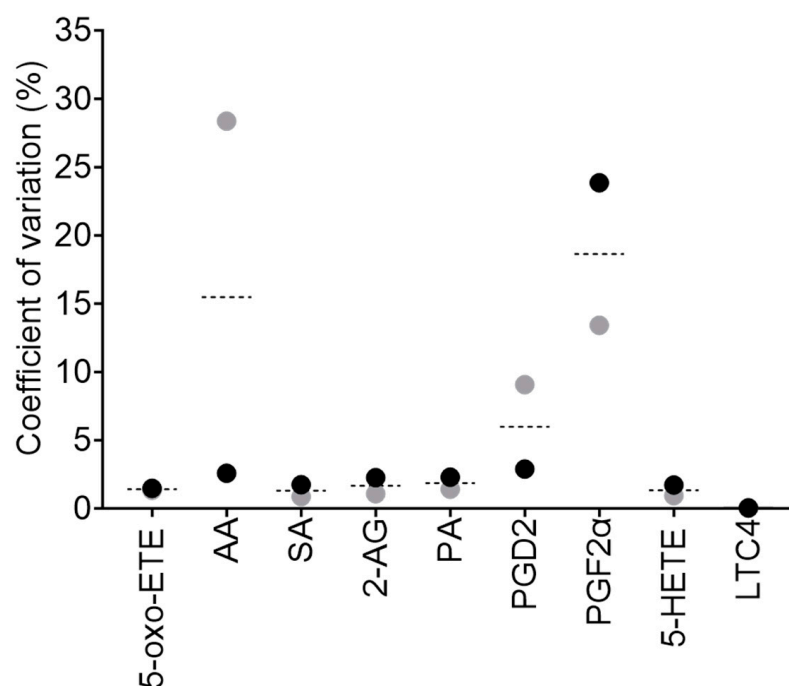


Figure 2. Method reproducibility (intraday analysis). Lipid standards were combined and analysed in technical triplicate at two concentrations, 0.3 pmol (grey dots) and 3 pmol (black dots) on-column, respectively. The CV between technical triplicates was calculated (as %) for each standard, as a mean of the two concentrations (dashed line) or individually (dots).

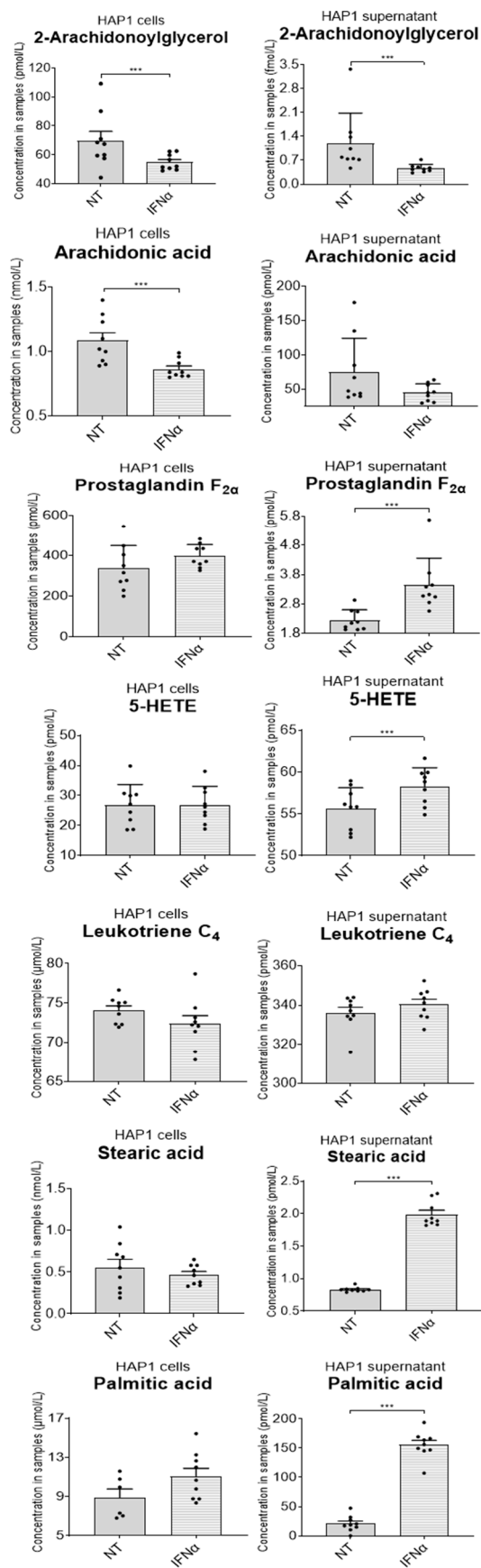
2.2. Bioactive Lipid Analysis in Biological Samples

To enhance the extraction of lipids from cells, three different liquid–liquid extraction (LLE) techniques were tested (Figure S2a). The bioactive lipid mix (BLM, see Section 4.3. Standard Solutions), containing all the lipid standards of interest, was added to cells in the extraction buffer to yield a final concentration of 10 pmol/L on column. We established that Extraction 1 was the most optimal extraction method for PGD₂, and Extraction 3 was optimal for extracting 2-AG, AA and LTC₄. However, Extraction 2 was ideal for the majority of metabolites (5-HETE, 5-oxo-ETE, PA, PGF₂α and SA) (Figure S2b and Table S1a) and therefore it was the method of choice for the lipid extraction from cells in subsequent experiments. Metabolite extraction from the media in which the cells were cultured (the cell supernatant) was performed in a similar manner to the metabolite extraction from cells, with the exception that steps 1 and 2 were combined (Figure S3a). We determined that Extraction 1 was the most optimal extraction method for 2-AG and LTC₄, and Extraction 2 was most optimal for the extraction of 5-HETE, AA and 5-oxo-ETE (Figure S3b and Table S1b). Extraction 3 resulted in the extraction of all lipids, with the highest extraction efficiency for four of the nine lipids analysed (PA, PGF₂α, PGD₂/E₂ and SA), and therefore it was the method of choice for lipid extraction from cell supernatant samples in subsequent experiments.

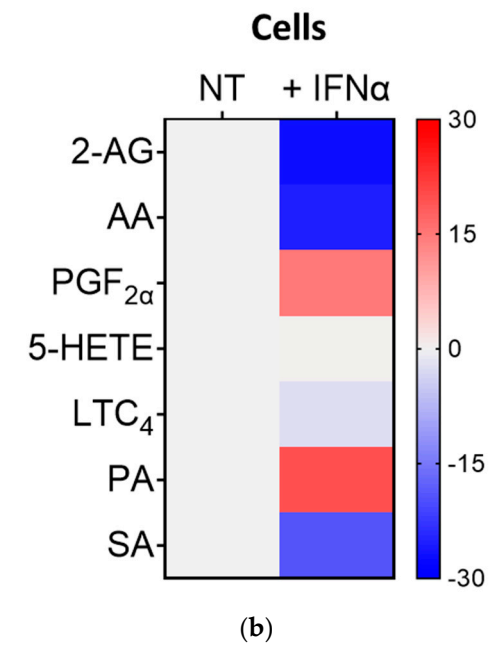
We subsequently determined the matrix effect for cell and cell supernatant samples (see Section 4.7. Data Analysis), to evaluate whether the complex biological mixture enhances or suppresses ionisation for each lipid, by calculating a corresponding matrix RF value (Figure S4), which ranged from 0.34 to 40.06 for cells and 0.07 to 4.81 for cell supernatants (Table S2). The high degree of variation in matrix RF values for each lipid highlights the importance of determining a matrix RF for every individual lipid analysed, in each specific sample type.

2.3. Analysis of the Bioactive Lipidome after IFN-I Treatment in Cancer Cells

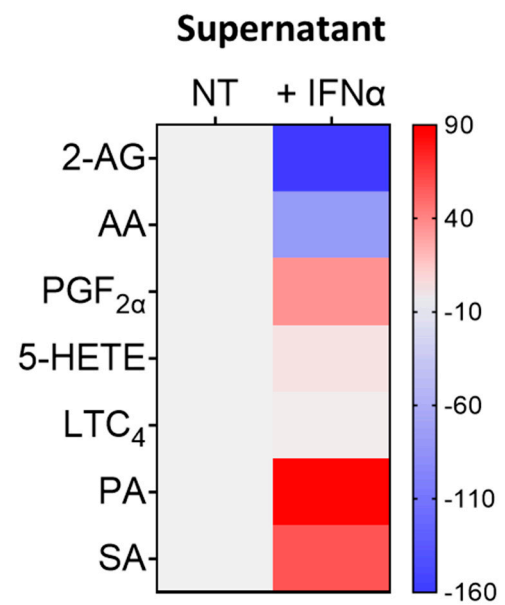
To validate our methodology, we decided to profile the nine lipids of interest in a CML-derived cell line, upon treatment with IFN-I. This treatment resulted in significant changes to the intracellular lipidome in cell samples (Figure 3a,b, Table S3a–d), as well as the extracellular lipidome in cell supernatant samples (Figure 3a,c, Table S4a–d). We observed a decrease in the intra- and extracellular concentrations of 2-AG upon IFN-I treatment, and a similar decrease was seen in intracellular concentrations of AA, which was in line with data published in literature [39]. Although we cannot confidently say whether this was due to a decrease in the synthesis of these lipids or an increase in their degradation, their increased conversion into downstream lipid metabolites upon IFN-I treatment is another plausible mechanism. An increase in the extracellular levels of $\text{PGF}_{2\alpha}$ was observed, and the intracellular concentrations of 5-HETE did not change upon IFN-I treatment. This suggests that 2-AG and AA may be used to generate 5-HETE in the presence of IFN-I. There was no significant change in LTC_4 in cells or in the cell supernatant, indicating no major changes in the synthesis or usage of this lipid. Intracellular amounts of PA and SA were not affected. However, extracellular amounts of PA and SA increased significantly. This would suggest an increase in the synthesis and secretion of these fatty acids. 5-oxo-EETE, PGD_2 and PGE_2 were not identified in either cell or cell supernatant fractions. Nonetheless, this method can be used to confidently detect minute changes for all these lipids (even if the changes are not statistically significant). The overall change in the bioactive lipid profile after a 36 h IFN-I treatment is shown in Figure 3d.



(a)



(b)



(c)

Figure 3. Cont.

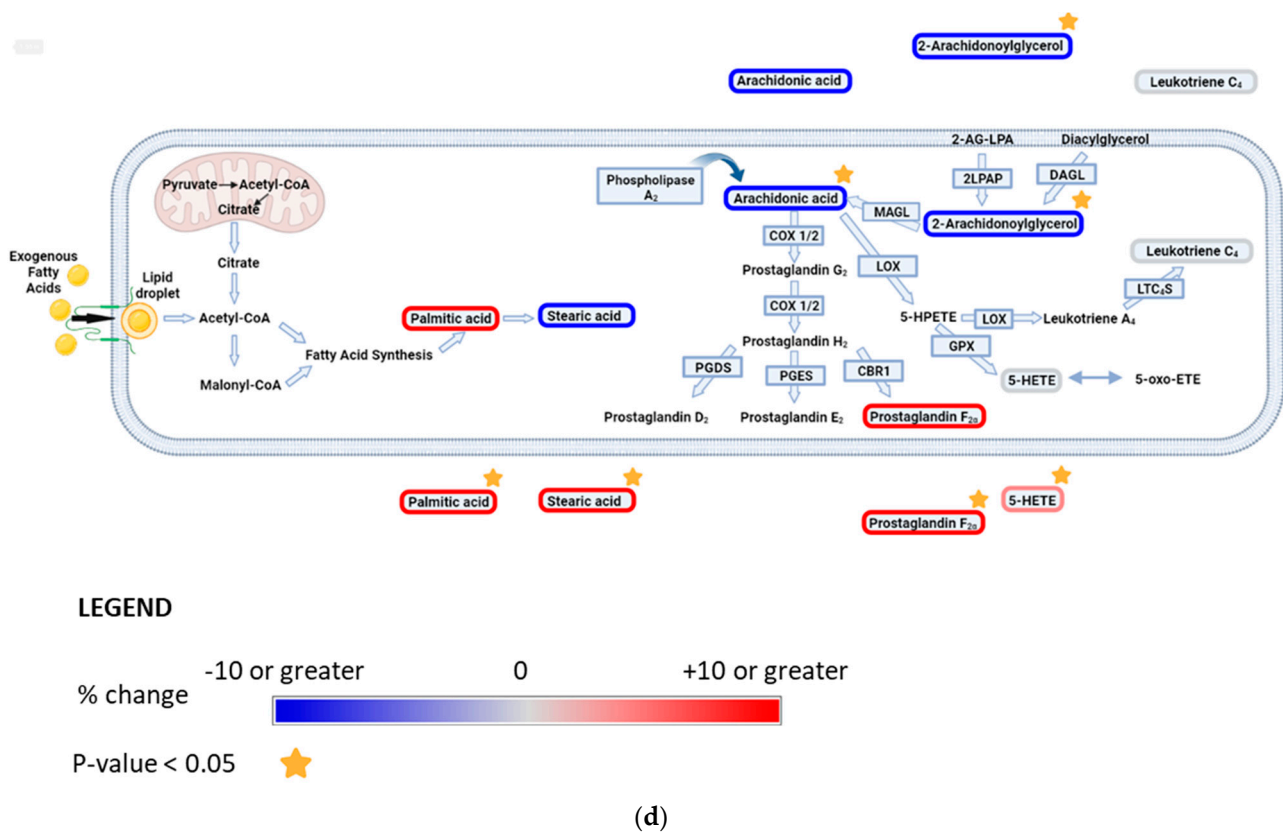


Figure 3. Interferon alpha modulates eicosanoid and fatty acid pathways. (a) Analysis of bioactive lipids in HAP1 cells and cell supernatants after 36 h treatment with IFN-I. (a) Graphs represent the mean with the standard error of the mean (SEM). Cell results are the graphs on the left; the corresponding cell supernatant is on the right. Grey bars are for the not-treated sample (NT) and grey bars with a white stripe pattern are the results for the IFN-I-treated samples. The statistical analysis is the two sample (or unpaired) *t*-test. A *p*-value less than 0.05 (***) suggests that the results have highly significant differences. If there is no significance difference, it is not labelled. (b) Mean percentage change of bioactive lipids in HAP1 cells, not-treated (NT) and treated with IFN α for 36 h (+IFN α). (c) Cell supernatant from HAP1 cells, not-treated (NT) and treated with IFN α for 36 h (+IFN α). Heat maps display normalised lipid abundances relative to the mean concentration of the non-treated samples (NT), which is represented by the grey bars. For IFN treatment, blue results are for a decrease in concentration, in percentage, grey is for no change and red is for an increase in concentration in percentage. (d) Bioactive lipid profile after 36 h treatment with IFN-I. Converting enzymes are in boxes and the lipids in this study are circled. Lipids circled in grey have no change compared to non-treated cells; lipids circled in blue have a decreased concentration compared to non-treated cells; and lipids circled in red have an increased concentration compared to non-treated cells. Lipids discovered in the cell supernatant are outside of the cell lipid membrane. Lipids with a significant difference between non-treated and treated (a *p*-value of less than 0.05) are indicated by a yellow star.

3. Discussion

The primary objective of this article was to optimise and implement a targeted lipidomics workflow in a disease-relevant cellular model to monitor the effects of an approved form of treatment. We have used HAP1 cells as a model for CML, as HAP1 cells are derived from CML patient cells and have the BCR-ABL gene, which is common in leukaemia's, turning the myeloid cell into a chronic myeloid cell [34,35], and IFN-I (IFN α 2) as a treatment. IFN-I is a currently used, alone and in combination with tyrosine kinase inhibitors (TKIs), form of treatment for CML in the clinics [38].

First, we have established the importance of investigating the appropriate extraction technique for the specific sample type (e.g., cells or cell supernatant). Second, we considered the matrix effect of every lipid analysed within the specific sample type.

Due to intrinsic molecular differences, innate variation and organic solvent preferences during extraction, there is no agreement on the best sample preparation and analysis of lipids. As a consequence, analysing different subclasses simultaneously is challenging. In this study, we have optimised extraction, chromatography and MS parameters, which provide the best conditions for the identification and quantitation of a set of eicosanoids and fatty acids with well-established roles in inflammation.

Solid-phase extraction (SPE) methods can be used to reduce the complexity, and to concentrate the samples, prior to analysis. However, we found that SPE is unreliable for concentrating a variety of lipids simultaneously, resulting in the loss of some metabolites (unpublished observations). Therefore, we opted to optimise LLE methods and concentrate samples subsequently by resuspension of the dried lipids into smaller volumes. Due to differences in the natural abundance of these metabolites, and the MS response, we were able to dilute the sample for those lipids with a higher natural concentration and/or a higher ion intensity (such as intracellular 2-AG). A separate method could be implemented for the analysis of 2-AG, LTC₄ and PGF_{2 α} , as even at low on-column concentrations these lipids have a large AUC. For instance, the standards and samples could be diluted further than reported here. Pre-analytical influences may change lipid concentrations or matrices, which is why we prefer to use extensive matrix-dependent normalisations for each analyte within a “true” matrix (e.g., not a surrogate matrix), and demonstrate its application tailored to specific endogenous lipid (eicosanoids and fatty acids) detection in clinically relevant biological samples. However, to bypass normalisation calculations, to provide information on the regulatory network and to identify important metabolite conversions within the pathway, ratios between metabolites could be used instead (e.g., PGE₂:PGF_{2 α}). In this analysis, there is variability in response curves for the lipids (R^2 values from 0.950 to 0.999; Table S5 and Figure S5), and variation in the matrix effects (RF values from 0.34 to 40.06), highlighting the need to determine the responses for every lipid quantified, as the results would otherwise vary significantly from the observed amounts. Nonetheless, the reproducibility of detection for our method achieved technical CV values of less than 20% and were within 5–10% for most species (Figure 2). Our intraday variation for all lipids analysed was below 20% CV, with 5-oxo-EETE, SA, 2-AG, PA and 5-HETE being below 5%.

Recommended options for the future development of this analysis could include chemical derivatisation of the lipids, exploring an analysis in negative mode electrospray ionisation (ESI[−]), using an ultrafast LC and a complementary proteomics analysis. Derivatization has been implemented for enhanced lipidomic analysis by MS [40], and it may boost the MS response for some lipids. However, it would need to be considered that derivatization itself is laborious and time-consuming, that different metabolites have differing derivatization efficiencies and that batch effects are common. It has also been described that lipids with carboxylic acid moieties will benefit from being analysed in negative polarity [41,42]. However, this may not be suitable for the simultaneous analysis of all the lipids reported here. For instance, and in line with our observations, ionisation of LTC₄ has been already shown to be very efficient in positive polarity [43]. MS fast-switching between polarity modes could potentially further improve the sensitivity of detection. It is important to consider that PUFAs are easily oxidised and that this may lead to erroneous concentration reporting for some lipids. Using an ultrafast LC could reduce the total analysis time, increasing throughput and reducing the cost per sample and labour time (samples would not need to be added daily). In addition, sample quality could be improved as they would not need to be stored for as long in the autosampler. Integrating complementary proteomics data would lead to greater understanding and enhance confidence in the changes observed within the studied pathways. For instance, changes in the expression of some of the enzymes involved in the metabolism of eicosanoids and fatty acids have been associated with cancer development [44–47]. Pinpointing which enzymes are modified

upon interferon treatment, using proteomics, may corroborate our findings and expand our knowledge of the effect of interferon treatment in CML patients.

The pro-inflammatory tumour microenvironment [37,48–51] and immune “hot” tumours show increased levels of inflammation and anticancer immune responses, such as T cell infiltration and the release of pro-inflammatory cytokines, including interferons. Defects in interferon signalling pathways during cancer treatment have been linked to immunotherapy resistance [52]. Our results suggest that IFN-I treatment significantly reduces the intracellular concentration of the eicosanoid precursors 2-AG and AA. However, the underlying molecular mechanism is as yet still unknown. We hypothesise that this reduction may be through decreased production of their precursors (2-AG-LPA or DAG), a decreased presence or activity of the respective enzymes which produce 2-AG-LAP and DAG (for example, 2-LPAP or DAGL) or by increased metabolism to downstream eicosanoids (such as PGF_{2α}). The latter seems to be the case as both intracellular and extracellular concentrations of PGF_{2α} are increasing. This may suggest that cells treated with IFN-I are secreting excess PGF_{2α} out of the intracellular space. Increased concentrations of PGF_{2α} have been indicated as a driver of particular cancers [53–55], although its role in CML remains unclear. Secretion of SA and PA also appear increased upon IFN-I exposure, possibly through enhanced export. These fatty acids could contribute to the tumour microenvironment, act as key metabolites in reducing tumourigenicity and affect the interplay between tumour and immune cells. 5-oxo-ETE, PGD₂ and PGE₂ were not identified in the samples, indicating either their absence, that they fell below the lower limit of detection (LLOD, a signal-to-noise ratio of >3), and/or the matrix caused considerable ionisation suppression. Alternatively, perhaps there was unexpected in-source fragmentation, leading to differing parent or product ions from those that we monitored. 5-oxo-ETE could be rapidly metabolised to either 5-HETE or to Di-endoperoxidase [56,57], and therefore with the current treatment of 36 h it is very likely that the changes, if happening upon IFN-I treatment, will not be observed.

We were unable to chromatographically separate standards of the isobaric species PGD₂ and PGE₂. However, separation is possible with a method specifically dedicated to the analysis of these particular lipids. Employing normal-phase chiral chromatography, and/or alternative MS approaches (employing additional separation techniques, such as ion mobility), will isolate isobaric prostaglandins based on their chirality, mobility and/or collisional cross-section value. PGD₂ can undergo dehydration to form Prostaglandin J₂, and other Prostaglandin metabolites, with the dehydration of PGD₂ being accelerated in the presence of serum albumin [58–60]. Since our tissue culture medium contains serum albumin, it might be contributing to the absence of PGD₂ in our analysis. Previous studies have suggested that PGE₂ is reduced in CML patients [61]; hence, this may be why our method was unable to detect PGE₂ in samples. Upon IFN treatment, intracellular production of 5-HETE appears to be maintained, possibly through metabolism from AA, or by the reduction of 5-oxo-ETE (and NADP⁺) to 5-HETE (and NADPH) [57]. In addition, the extracellular quantity of 5-HETE significantly increases, which to our knowledge is novel biology and an area of CML research yet to be explored. Changes in LTC₄ amount and activity, and LTC₄ concentration, are cell-specific [62–64]. With CML researchers suggesting that there can be a steady state, an increase or a decrease in Leukotrienes in patients compared to healthy controls. Nonetheless, despite these disparities, inhibitors of Leukotriene signalling have reduced cancer growth in CML [65,66]. When these Leukotriene inhibitors have been used in combination with traditional methods to treat CML (tyrosine kinase inhibitors), the reduction in tumour growth was further increased [67]. Interestingly, our results, although not significant, show a slight decrease in intracellular LTC₄ levels upon IFN-I stimulation. However, Leukotrienes can be readily metabolised [68], with LTC₄ potentially being converted to Leukotriene D₄; therefore, we cannot confirm that LTC₄ concentrations are affected or not by 36 h of IFN-I treatment.

In conclusion, the present study describes an original, ultra-sensitive methodology, whereby LC and MS parameters were adapted to a specific set of lipids. Protocols for

extracting these lipids from different sample types were modified considering the matrix effect of each individual lipid as well as the different sample types (cells and cell supernatant). We applied this workflow for an accurate and simultaneous analysis of a range of eicosanoids and fatty acids in a clinically relevant cellular model of CML. It would be interesting, in order to reflect the heterogeneity and diversity of CML patients, to analyse, using this analytical workflow, cells and cell supernatants from different CML cell lines, with different genetic backgrounds and, ideally, from primary cells representing the different subtypes of CML. This would include the lipidome analysis of patient samples with either the Philadelphia chromosome or the Bcr-Abl oncogene, at Chronic, Accelerated and Blast phases of CML. Our optimisation of sample preparation, technical parameters and data normalisation for different sample types, plus the application of dMRM transitions, maximises the sensitivity of detection, allowing detection at endogenous levels, even for very-low-abundance species. The observed improvements in detection and sensitivity are the hallmark of this analytical method, permitting us to resolve changes in relevant bioactive lipids in response to treatment with a pro-inflammatory cytokine in a cancer cell model. Translational application examples include the profiling of bioactive lipids in patient samples, for monitoring inflammation levels caused by pathology, or for treatment with immunomodulators (i.e., immunotherapy). In closing, we believe that this emphasises the benefits of using targeted MS in understanding pathophysiological states.

4. Materials and Methods

4.1. Figures

Figures 1a,b, 3d, S2a, S3a and S4 were generated in Biorender.

4.2. Reagents

Lipid standards: PGE₂ (catalogue # sc-201225), PGF_{2α} (catalogue # sc-201227), 5-HETE (catalogue # sc-205136), 5-oxo-EETE (catalogue # sc-203783) and PGD₂ (catalogue # sc-201221) were purchased from Santa Cruz Biotechnology (Dallas, TX, USA). SA (catalogue # 10011298–500 mg-CA), LTC₄ (catalogue # 20210–25 ug-CAY) and PA (catalogue # 10006627-10 g-CAY) were acquired from Cayman Chemicals (Ann Arbor, MI, USA). AA (catalogue # ab120916) is from Abcam (Cambridge, UK). 2-AG (catalogue # A8973) was purchased from Sigma (St. Louis, MO, USA). LC-MS grade water (Catalogue # 115333) and MeOH (Catalogue # 106035) were available from Merck (Lowe, NJ, USA). Ammonium acetate (Catalogue # 10365260) and IPA (Catalogue # 15686670) were from Fisher Scientific (Waltham, MA, USA). MTBE was acquired from Acros organics (Catalogue # 3787 20010) and ACN was from Honeywell Riedel-de Haën (York, UK) (Catalogue # 348512.5L). IMDM was from Gibco (Billings, MT, USA) at Thermo Fisher Scientific (reagent # 12440053) and IFN-I was from Biotechne R&D systems (Minneapolis, MN, USA) (catalogue # 11105-1).

4.3. Standard Solutions

Stock concentrations of all lipid standards were prepared as individual aliquots at 100 μmol/L in 100% MeOH. These stocks were then pooled and serially diluted to a concentration of 100 nmol/L in 50% (*v/v*) MeOH to create an equimolar standard mixture, the bioactive lipid mix (BLM). The BLM was used as a spike, which was added to pooled samples (a fraction of all samples combined) to determine the matrix effects.

4.4. Tissue Culture

HAP1 cells were cultured as previously described [69]. In brief, cells were cultured in IMDM media containing 10% FBS and grown until 60–70% confluence. Cells were then treated with 1000 U/mL of IFNα-2b for 36 h, until ~80% confluent. The surrounding medium (the cell supernatant) was collected and used for analysis of extracellular lipids. Both cell supernatant and cell plates were stored at –80 °C until lipid extraction.

4.5. Lipid Extraction

A simultaneous lysis and LLE was performed. For cells, the lysis was performed by scraping with 100% MeOH. The lysate was then added to 50% CHCl₃ and 50% MBTE, which was then vortexed briefly and then spun at 12 rpm for 20 min at 4 °C. The sample was then centrifuged at 17× *g* for 5 min at 4 °C and the resulting organic fraction was removed and stored on ice. The remaining pellet underwent another round of vortexing, spinning and centrifuging in 50% CHCl₃ and 50% MTBE, with the resulting organic fraction being pooled with the previous fraction. The final extraction step was performed with 50% MeOH and the sample was vortexed, spun and centrifuged again, with the organic fraction being pooled with the previous fractions. Once all organic fractions were collected for each sample, a small portion of each was removed and pooled together for a pooled sample. The samples and the pooled samples were then dried in a speedvac at 30 °C until dry and then stored at −20 °C until LC-MS analysis.

To the dried lipid extracts 50% MeOH or the same volume of the BLM was added prior to analysis. The samples were briefly vortexed and then shaken at 400 rpm at 4 °C until homogenous. Cell supernatant samples were diluted 1 in 20. Cell samples were diluted 1 in 10 for analysis of AA, PGF_{2α}, SA and 5-HETE or diluted 1 in 100 for analysis of 2-AG, PA and LTC₄. Diluted samples were then transferred to LC-MS autosampler vials.

4.6. LC-MS Method

Levels of 2-AG, AA, PGD₂, PGE₂, PGF_{2α}, 5-HETE, 5-oxo-EETE, LTC₄, PA and SA were analysed. Metabolites were quantified using an optimised dMRM method on a triple quadrupole mass spectrometer with a JetStream ESI source (Agilent 6490) coupled to a 1290 Agilent LC system.

Lipids were separated on an ACQUITY UPLC BEH C18 column (1.7 μm, 100 × 2.1 mm i.d., Waters) with mobile phase A of 2% IPA with 5 mM ammonium acetate and mobile phase B of 100% IPA with 5 mM ammonium acetate at 40 °C. The flow rate was set to 0.21 mL min^{−1} and the sample injection volume was 1 μL, 10 μL or 15 μL (depending on the response of the metabolites). The following gradient (% mobile phase B) was used: 0–1.5 min at 50% B, 1.5–9 min 70% B and 9–13 min 100% B. A wash with 100% mobile phase B and a wash with 100% mobile phase A were performed to clean the column before re-equilibration to starting conditions. The autosampler was maintained at 4 °C.

The following ESI+ source parameters were used: gas temp at 280 °C, gas flow 14 L/min, nebuliser at 20 psi, sheath gas temp at 250 °C, sheath gas flow at 11 L/min, capillary voltage 3000 V, nozzle voltage 1500 V, high-pressure RF at 150 V and low-pressure RF at 60 V. The transitions used in the dMRM analysis are shown in Table 1; the LC and MS parameters used are shown in Table 2.

4.7. Data Analysis

Initial data processing was performed using Agilent MassHunter Quantitative Analysis software (v. 10). Post-processing was performed in Excel and GraphPad Prism 9.2.0.

The MRM AUCs were corrected with the matrix response factor (matrix RF) (Figure S4). To determine the matrix RF, the response of the analyte as a standard is needed, as is the response in the sample (the intrinsic contribution, the matrix) and the response of the standard mixture spiked into the matrix. To calculate the matrix RF, the response of the intrinsic contribution in the sample (the matrix) is subtracted from the response of the standard mixture spiked into the matrix, to give the effect of the matrix upon the standard (response of the standard mixture in the matrix). The response of the standard by itself divided by the response of the standard mixture in the matrix gives a matrix response factor.

To account for matrix effects in biological samples, the response of an analyte in a (biological) sample is multiplied by the corresponding matrix RF value to give the “real” response of the analyte (i.e., to eliminate ionisation enhancement/suppression effects on an analyte). This matrix RF-corrected response can subsequently be used to calculate analyte

concentration from a standard curve trendline equation ($y = Mx + C$). Standard curves are generated by the injection of increasing concentrations of the BLM, calculating the AUC at each concentration, and plotting AUC values against the corresponding concentration.

Statistical analysis of the two sample (or unpaired) *t*-test is used to validate difference between no treatment (NT) and treated with IFN α (+IFN α) for 36 h. A *p*-value less than 0.05 (***) indicates that the results have highly significant differences.

4.8. Method Validation

The LLOD was calculated as a S/N ratio of >3; the lower limit of quantification (LLOQ) was a S/N ratio of >10. Intraday precision was calculated using three replicates of two concentrations over the course of one day and the results are reported as CV % between replicates of one concentration. To monitor instrument performance over time and check that batches that spanned interday analysis were consistent (quality control, QC), the BLM (1 pmol/L on-column) was routinely injected. If the total sample analysis time was over multiple days, the samples were briefly vortexed at the start of each day to avoid precipitation.

Supplementary Materials: The supporting information can be downloaded at: <https://www.mdpi.com/article/10.3390/ijms242115513/s1>.

Author Contributions: Conceptualisation and writing—original draft preparation, H.C.S., B.M.K. and A.P.-F.; methodology, validation, formal analysis and visualisation, H.C.S.; software and data curation, H.C.S. and Z.Y.; investigation, H.C.S., S.D.D. and A.P.-F.; resources, supervision, project administration and funding acquisition, B.M.K. and A.P.-F.; writing—review and editing, H.C.S., S.D.D., Z.Y., B.M.K. and A.P.-F. All authors have read and agreed to the published version of the manuscript.

Funding: H.C.S., S.D.D., Z.Y., B.M.K. and A.P.F. are funded by the Chinese Academy of Medical Sciences (CAMS) Innovation Fund for Medical Science (CIFMS), China (grant nr—2018-I2M-2-002). H.C.S., S.D.D., B.M.K. and A.P.F. are also funded by Pfizer Inc.

Data Availability Statement: Data have been submitted to the public repository metabolomeXchange (Metabolights), reference MTBLS7875.

Acknowledgments: Many thanks to Alan Scott for reviewing the text prior to publication. We would also like to thank Paolo Spingardi (UCL Business Ltd.) and Ashvina Segaran (Ludwig Cancer Research, University of Oxford) for their assistance in the operation and maintenance of the triple quad mass spectrometer, and for their helpful insights into method optimisation.

Conflicts of Interest: The authors declare no conflict of interest.

Abbreviations

2-AG; 2-Arachidonoylglycerol, 2-AG-LPA; 2-Arachidonoylglycerol lysophosphatidic acid, 2LPAP; 2-Lysophosphatidic acid phosphatase, 5-HETE; 5-Hydroxyeicosatetraenoic acid, 5-HPETE; 5-Hydroperoxyeicosatetraenoic acid, 5-oxo-EETE; 5-Oxo-eicosatetraenoic acid, AA; Arachidonic Acid, ACN: Acetonitrile, AUC; area under the curve, BLM; bioactive lipid mix, CBR1; Carbonyl reductase 1, CE; collisional energy, CHCl₃; chloroform, CML; chronic myeloid leukaemia, COX 1/2; Cytochrome C oxidase 1 or 2, CV; coefficient of variation, DAGL; Diacylglycerol lipase, dMRM; dynamic multiple reaction monitoring, ESI; electrospray ionisation, eV; electron volts, FBS; foetal bovine serum, GPX; Glutathione peroxidase, H₂O; water, HMDB; Human Metabolome Database, IFN α ; interferon alpha, IMDM; Iscove's Modified Dulbecco's Medium, IPA; isopropanol, LC-MRM-QQQ; liquid chromatography–multiple reaction monitoring–triple quadrupole, LC-MS; liquid chromatography–mass spectrometry, LLE; liquid–liquid extraction, LLOD; lower limit of detection, LLOQ; lower limit of quantification, LOX; Lysyl Oxidase, LTA₄; Leukotriene A₄, LTC₄; Leukotriene C₄, LTC₄S; Leukotriene C₄ synthase, LTC₄S; LTC₄ synthase, m/z; mass-to-charge ratio, MAGL; Monoacylglycerol lipase, MeOH; Methanol, MRMHR; multiple reaction monitoring high-resolution, MTBE; Methyl tert-butyl ether, NADP⁺/NADPH; nicotinamide adenine dinucleotide phosphate, NT; non-treated, PA; Palmitic acid, PGD₂; Prostaglandin D₂, PGDS; Prostaglandin D₂ synthase, PGE₂; Prostaglandin

E₂, PGES; Prostaglandin E₂ synthase, PGF_{2α}; Prostaglandin F_{2α}, PUFAs; polyunsaturated fatty acids, QC; quality control, QTOF; quadrupole time of flight, RF; response factor, SD; standard deviation, S/N; signal-to-noise ratio, SA; Stearic acid, SPE; solid-phase extraction, TIMS-TOF; trapped ion mobility–time of flight, UPLC-MS/MS; ultra-performance liquid chromatography–tandem mass spectrometry.

References

1. Wang, C.; Yang, J.; Zhang, X. Editorial: The Role of Bioactive Lipids in Homeostasis and Pathology. *Front. Physiol.* **2021**, *12*, 773632. [[CrossRef](#)] [[PubMed](#)]
2. Minhas, P.S.; Latif-Hernandez, A.; McReynolds, M.R.; Durairaj, A.S.; Wang, Q.; Rubin, A.; Joshi, A.U.; He, J.Q.; Gauba, E.; Liu, L.; et al. Restoring metabolism of myeloid cells reverses cognitive decline in ageing. *Nature* **2021**, *590*, 122–128. [[CrossRef](#)] [[PubMed](#)]
3. Lindqvist, H.M.; Winkvist, A.; Gjertsson, I.; Calder, P.C.; Armando, A.M.; Quehenberger, O.; Coras, R.; Guma, M. Influence of Dietary n-3 Long Chain Polyunsaturated Fatty Acid Intake on Oxylipins in Erythrocytes of Women with Rheumatoid Arthritis. *Molecules* **2023**, *28*, 717. [[CrossRef](#)] [[PubMed](#)]
4. Zhou, Y.J.; Wang, J.H.; Li, L.; Yang, H.W.; Wen, D.L.; He, Q.C. Expanding expression of the 5-lipoxygenase/leukotriene B₄ pathway in atherosclerotic lesions of diabetic patients promotes plaque instability. *Biochem. Biophys. Res. Commun.* **2007**, *363*, 30–36. [[CrossRef](#)] [[PubMed](#)]
5. Cipollone, F.; Mezzetti, A.; Fazio, M.L.; Cucurullo, C.; Iezzi, A.; Uchino, S.; Spigonardo, F.; Bucci, M.; Cucurullo, F.; Prescott, S.M.; et al. Association between 5-lipoxygenase expression and plaque instability in humans. *Arter. Thromb. Vasc. Biol.* **2005**, *25*, 1665–1670. [[CrossRef](#)]
6. Zu, L.; Guo, L.; Zhou, B.; Gao, W. Relationship between metabolites of arachidonic acid and prognosis in patients with acute coronary syndrome. *Thromb. Res.* **2016**, *144*, 192–201. [[CrossRef](#)] [[PubMed](#)]
7. Chang, N.; Wu, C.; Chen, D.; Yeh, C.; Lin, C. High levels of arachidonic acid and peroxisome proliferator-activated receptor-α in breast cancer tissues are associated with promoting cancer cell proliferation. *J. Nutr. Biochem.* **2013**, *24*, 274–281. [[CrossRef](#)]
8. Rolland, P.H.; Martin, P.M.; Jacquemier, J.; Rolland, A.M.; Toga, M. Prostaglandin in human breast cancer: Evidence suggesting that an elevated prostaglandin production is a marker of high metastatic potential for neoplastic cells. *J. Natl. Cancer Inst.* **1980**, *64*, 1061–1070.
9. Sipka, S.; Szántó, S.; Szucs, K.; Kovács, I.; Kiss, E.; Antal-Számás, P.; Lakos, G.; Aleksza, M.; Illés, A.; Gergely, P.; et al. Decreased arachidonic acid release in peripheral blood monocytes of patients with systemic lupus erythematosus. *J. Rheu-Matol.* **2001**, *28*, 2012–2017.
10. Prüss, H.; Rosche, B.; Sullivan, A.B.; Brommer, B.; Wengert, O.; Gronert, K.; Schwab, J.M. Proresolubilization lipid mediators in multiple sclerosis—differential, disease severity-dependent synthesis—A clinical pilot trial. *PLoS ONE* **2013**, *8*, e55859. [[CrossRef](#)]
11. Sacerdoti, D.; Balazy, M.; Angeli, P.; Gatta, A.; McGiff, J.C. Eicosanoid excretion in hepatic cirrhosis. *J. Clin. Investig.* **1997**, *100*, 1264–1270. [[CrossRef](#)]
12. Martín-Masot, R.; Galo-Licon, J.D.; Mota-Martorell, N.; Sol, J.; Jové, M.; Maldonado, J.; Pamplona, R.; Nestares, T. Up-Regulation of Specific Bioactive Lipids in Celiac Disease. *Nutrients* **2021**, *13*, 2271. [[CrossRef](#)] [[PubMed](#)]
13. Kathir, K.; Dennis, J.M.; Croft, K.D.; Mori, T.A.; Lau, A.K.; Adams, M.R.; Stocker, R. Equivalent lipid oxidation profiles in advanced atherosclerotic lesions of carotid endarterectomy plaques obtained from symptomatic type 2 diabetic and nondiabetic subjects. *Free Radic. Biol. Med.* **2010**, *49*, 481–486. [[CrossRef](#)] [[PubMed](#)]
14. Zakrzewski, J.T.; Barnes, N.C.; Piper, P.J.; Costello, J.F. Detection of sputum eicosanoids in cystic fibrosis and in normal saliva by bioassay and radioimmunoassay. *Br. J. Clin. Pharmacol.* **1987**, *23*, 19–27. [[CrossRef](#)]
15. Minuz, P.; Jiang, H.; Fava, C.; Turolo, L.; Tacconelli, S.; Ricci, M.; Patrignani, P.; Morganti, A.; Lechi, A.; McGiff, J.C. Altered release of cytochrome p450 metabolites of arachidonic acid in renovascular disease. *Hypertension* **2008**, *51*, 1379–1385. [[CrossRef](#)] [[PubMed](#)]
16. Lundström, S.L.; Levänen, B.; Nording, M.; Klepczynska-Nyström, A.; Sköld, M.; Haeggström, J.Z.; Grunewald, J.; Svartengren, M.; Hammock, B.D.; Larsson, B.; et al. Asthmatics exhibit altered oxylipin profiles compared to healthy individuals after subway air exposure. *PLoS ONE* **2011**, *6*, e23864. [[CrossRef](#)]
17. Chiurchiù, V.; Leuti, A.; Maccarrone, M. Bioactive Lipids and Chronic Inflammation: Managing the Fire Within. *Front. Immunol.* **2018**, *9*, 38. [[CrossRef](#)]
18. Amine, H.; Benomar, Y.; Taouis, M. Palmitic acid promotes resistin-induced insulin resistance and inflammation in SH-SY5Y human neuroblastoma. *Sci. Rep.* **2021**, *11*, 5427. [[CrossRef](#)]
19. Anderson, E.K.; Hill, A.A.; Hasty, A.H. Stearic acid accumulation in macrophages induces toll-like receptor 4/2-independent inflammation leading to endoplasmic reticulum stress-mediated apoptosis. *Arter. Thromb. Vasc. Biol.* **2012**, *32*, 1687–1695. [[CrossRef](#)] [[PubMed](#)]

20. Guo, B.; Chen, B.; Liu, A.; Zhu, W.; Yao, S. Liquid chromatography-mass spectrometric multiple reaction monitoring-based strategies for expanding targeted profiling towards quantitative metabolomics. *Curr. Drug Metab.* **2012**, *13*, 1226–1243. [[CrossRef](#)] [[PubMed](#)]
21. Edwards, M.E.; De Luca, T.; Ferreira, C.R.; Collins, K.S.; Eadon, M.T.; Benson, E.A.; Sobreira, T.J.P.; Cooks, R.J. Multiple reaction monitoring profiling as an analytical strategy to investigate lipids in extracellular vesicles. *J. Mass Spectrom.* **2021**, *56*, e4681. [[CrossRef](#)]
22. Valli, A.; Rodriguez, M.; Moutsianas, L.; Fischer, R.; Fedele, V.; Huang, H.-L.; Van Stiphout, R.; Jones, D.; McCarthy, M.; Vinaxia, M.; et al. Hypoxia induces a lipogenic cancer cell phenotype via HIF1 α -dependent and -independent pathways. *Oncotarget* **2015**, *6*, 1920–1941. [[CrossRef](#)]
23. Cajka, T.; Fiehn, O. Comprehensive analysis of lipids in biological systems by liquid chromatography-mass spectrometry. *Trends Anal. Chem.* **2014**, *61*, 192–206. [[CrossRef](#)] [[PubMed](#)]
24. Kortz, L.; Dorow, J.; Ceglarek, U. Liquid chromatography-tandem mass spectrometry for the analysis of eicosanoids and related lipids in human biological matrices: A review. *J. Chromatogr. B Anal. Technol. Biomed. Life Sci.* **2014**, *964*, 1–11. [[CrossRef](#)] [[PubMed](#)]
25. Deems, R.; Buczynski, M.W.; Bowers-Gentry, R.; Harkewicz, R.; Dennis, E.A. Detection and quantitation of eicosanoids via high performance liquid chromatography-electrospray ionization-mass spectrometry. *Methods Enzymol.* **2007**, *432*, 59–82. [[CrossRef](#)]
26. Wang, Y.; Armando, A.M.; Quehenberger, O.; Yan, C.; Dennis, E.A. Comprehensive ultra-performance liquid chromatographic separation and mass spectrometric analysis of eicosanoid metabolites in human samples. *J. Chromatogr. A* **2014**, *1359*, 60–69. [[CrossRef](#)]
27. Lu, L.; Mai, Z.; Zhou, H.; Guan, W.; Wu, S.; Zou, H.; Shen, M.; Zhan, Y.; Ye, F.; Qiu, M.; et al. Simultaneous profiling and quantification of 25 eicosanoids in human serum by ultrahigh-performance liquid chromatography coupled to tandem mass spectrometry. *Anal. Bioanal. Chem.* **2022**, *414*, 8233–8244. [[CrossRef](#)]
28. Sorgi, C.A.; Peti, A.P.F.; Petta, T.; Meirelles, A.F.G.; Fontanari, C.; de Moraes, L.A.B.; Faccioli, L.H. Comprehensive high-resolution multiple-reaction monitoring mass spectrometry for targeted eicosanoid assays. *Sci. Data* **2018**, *21*, 180167. [[CrossRef](#)]
29. Miller, T.M.; Poloyac, S.M.; Anderson, K.B.; Waddell, B.L.; Messamore, E.; Yao, J.K. A rapid UPLC-MS/MS assay for eicosanoids in human plasma: Application to evaluate niacin responsiveness. *Prostaglandins Leukot. Essent. Fat. Acids* **2018**, *136*, 153–159. [[CrossRef](#)] [[PubMed](#)]
30. Raeven, P.; Hagn, G.; Niederstaetter, L.; Brugger, J.; Bayer-Blauensteiner, S.; Domenig, C.; Hoetzenecker, K.; Posch, M.; Leitner, G.; Gerner, C.; et al. Red blood cell transfusion-related eicosanoid profiles in intensive care patients—A prospective, observational feasibility study. *Front. Physiol.* **2023**, *14*, 1164926. [[CrossRef](#)] [[PubMed](#)]
31. Wang, D.; Pan, C.; Han, J.; Zhao, Y.; Liu, S.; Li, C.; Yi, Y.; Zhang, Y.; Tang, X.; Liang, A. Involvement of p38 MAPK/cPLA2 and arachidonic acid metabolic pathway in Shengmai injection-induced pseudo-allergic reactions. *J. Ethnopharmacol.* **2023**, *309*, 116357. [[CrossRef](#)] [[PubMed](#)]
32. Rustam, Y.H.; Reid, G.E. Analytical Challenges and Recent Advances in Mass Spectrometry Based Lipidomics. *Anal. Chem.* **2018**, *90*, 374–397. [[CrossRef](#)]
33. Murphy, R.C. Challenges in Mass Spectrometry-based Lipidomics of Neutral Lipids. *Trends Anal. Chem.* **2018**, *107*, 91–98. [[CrossRef](#)]
34. Heisterkamp, N.; Stam, K.; Groffen, J.; de Klein, A.; Grosveld, G. Structural organization of the bcr gene and its role in the Ph^t translocation. *Nature* **1985**, *315*, 758–761. [[CrossRef](#)] [[PubMed](#)]
35. Collins, S.J.; Kubonishi, I.; Miyoshi, I.; Groudine, M.T. Altered transcription of the c-abl oncogene in K-562 and other chronic myelogenous leukemia cells. *Science* **1984**, *225*, 72–74. [[CrossRef](#)] [[PubMed](#)]
36. Shen, H.; McHale, C.M.; Haider, S.I.; Jung, C.; Zhang, S.; Smith, M.T.; Zhang, L. Identification of Genes That Modulate Susceptibility to Formaldehyde and Imatinib by Functional Genomic Screening in Human Haploid KBM7 Cells. *Toxicol. Sci.* **2016**, *151*, 10–22. [[CrossRef](#)] [[PubMed](#)]
37. Aricò, E.; Castiello, L.; Capone, I.; Gabriele, L.; Belardelli, F. Type I Interferons and Cancer: An Evolving Story Demanding Novel Clinical Applications. *Cancers* **2019**, *11*, 1943. [[CrossRef](#)] [[PubMed](#)]
38. Paul, F.; Pellegrini, S.; Uzé, G. IFNA2: The prototypic human alpha interferon. *Gene* **2015**, *567*, 132–137. [[CrossRef](#)]
39. Want, E.J.; Masson, P.; Michopoulos, F.; Wilson, I.D.; Theodoridis, G.; Plumb, R.S.; Shockcor, J.; Loftus, N.; Holmes, E.; Nicholson, J.K. Global metabolic profiling of animal and human tissues via UPLC-MS. *Nat. Protoc.* **2013**, *8*, 17–33. [[CrossRef](#)] [[PubMed](#)]
40. Sun, D.; Meng, X.; Ren, T.; Fawcett, J.P.; Wang, H.; Gu, J. Establishment of a Charge Reversal Derivatization Strategy to Improve the Ionization Efficiency of Limaprost and Investigation of the Fragmentation Patterns of Limaprost Derivatives Via Exclusive Neutral Loss and Survival Yield Method. *J. Am. Soc. Mass Spectrom.* **2018**, *29*, 1365–1375. [[CrossRef](#)]
41. Kortz, L.; Dorow, J.; Becker, S.; Thiery, J.; Ceglarek, U. Fast liquid chromatography-quadrupole linear ion trap-mass spectrometry analysis of polyunsaturated fatty acids and eicosanoids in human plasma. *J. Chromatogr. B Anal. Technol. Biomed. Life Sci.* **2013**, *927*, 209–213. [[CrossRef](#)]
42. Song, J.; Liu, X.; Wu, J.; Meehan, M.J.; Blevitt, J.M.; Dorrestein, P.C.; Milla, M.E. A highly efficient, high-throughput lipidomics platform for the quantitative detection of eicosanoids in human whole blood. *Anal. Biochem.* **2013**, *433*, 181–188. [[CrossRef](#)]

43. Sanak, M.; Gielicz, A.; Bochenek, G.; Kaszuba, M.; Nizankowska-Mogilnicka, E.; Szczeklik, A. Targeted eicosanoid lipidomics of exhaled breath condensate provide a distinct pattern in the aspirin-intolerant asthma phenotype. *J. Allergy Clin. Immunol.* **2011**, *127*, 1141–1147.e2. [[CrossRef](#)] [[PubMed](#)]
44. Guzman, M. A new age for MAGL. *Chem. Biol.* **2010**, *17*, 4–6. [[CrossRef](#)]
45. Tuo, W.; Leleu-Chavain, N.; Spencer, J.; Sansook, S.; Millet, R.; Chavatte, P. Therapeutic potential of fatty acid amide hydrolase, monoacylglycerol lipase, and N-acyl ethanolamine acid amidase inhibitors. *J. Med. Chem.* **2017**, *60*, 4–46. [[CrossRef](#)]
46. Nomura, D.K.; Long, J.Z.; Niessen, S.; Hoover, H.S.; Ng, S.; Cravatt, B.F. Monoacylglycerol lipase regulates a fatty acid network that promotes cancer pathogenesis. *Cell* **2010**, *140*, 49–61. [[CrossRef](#)] [[PubMed](#)]
47. Giles, F.J.; Kantarjian, H.M.; Bekele, B.N.; Cortes, J.E.; Faderl, S.; Thomas, D.A.; Manshouri, T.; Rogers, A.; Keating, M.J.; Talpaz, M.; et al. Bone marrow cyclooxygenase-2 levels are elevated in chronic-phase chronic myeloid leukaemia and are associated with reduced survival. *Br. J. Haematol.* **2002**, *119*, 38–45. [[CrossRef](#)] [[PubMed](#)]
48. Stenke, L.; Sjölander, M.; Miale, T.D.; Lindgren, J.A. Novel enzymatic abnormalities in AML and CML in blast crisis: Elevated leucocyte leukotriene C4 synthase activity paralleled by deficient leukotriene biosynthesis from endogenous substrate. *Br. J. Haematol.* **1998**, *101*, 728–736. [[CrossRef](#)]
49. Cacho-Diaz, B.; García-Botello, D.R.; Wegman-Ostrosky, T.; Reyes-Soto, G.; Ortiz-Sánchez, E.; Herrera-Montalvo, L.A. Tumor microenvironment differences between primary tumor and brain metastases. *J. Transl. Med.* **2020**, *18*, 1. [[CrossRef](#)]
50. Roma-Rodrigues, C.; Mendes, R.; Baptista, P.V.; Fernandes, A.R. Targeting tumor microenvironment for cancer therapy. *Int. J. Mol. Sci.* **2019**, *20*, 840. [[CrossRef](#)]
51. Belli, C.; Trapani, D.; Viale, G.; D'Amico, P.; Duso, B.A.; Vigna, P.D.; Orsi, F.; Curigliano, G. Targeting the microenvironment in solid tumors. *Cancer Treat. Rev.* **2018**, *65*, 22–32. [[CrossRef](#)]
52. Nakamura, K.; Smyth, M.J. Targeting cancer-related inflammation in the era of immunotherapy. *Immunol. Cell Biol.* **2017**, *95*, 325–332. [[CrossRef](#)]
53. Kim, D.; Garza, L.A. A new target for squamous cell skin cancer? *Exp. Dermatol.* **2015**, *24*, 14–15. [[CrossRef](#)]
54. Pabst, T.; Kortz, L.; Fiedler, G.M.; Ceglarek, U.; Idle, J.R.; Beyoğlu, D. The plasma lipidome in acute myeloid leukemia at diagnosis in relation to clinical disease features. *BBA Clin.* **2017**, *7*, 105–114. [[CrossRef](#)] [[PubMed](#)]
55. Qualtrough, D.; Kaidi, A.; Chell, S.; Jabbour, H.N.; Williams, A.N.; Paraskeva, C. Prostaglandin F(2alpha) stimulates motility and invasion in colorectal tumor cells. *Int. J. Cancer* **2007**, *121*, 734–740. [[CrossRef](#)] [[PubMed](#)]
56. Griesser, M.; Boeglin, W.E.; Suzuki, T.; Schneider, C. Convergence of the 5-LOX and COX-2 pathways: Heme-catalyzed cleavage of the 5S-HETE-derived di-endoperoxide into aldehyde fragments. *J. Lipid Res.* **2009**, *50*, 2455–2462. [[CrossRef](#)] [[PubMed](#)]
57. Powell, W.S.; Gravelle, F.; Gravel, S.; Hashefi, M. Metabolism of 5(S)-hydroxyeicosanoids by a specific dehydrogenase in human neutrophils. *J. Lipid Mediat.* **1993**, *6*, 361–368.
58. Bie, Q.; Dong, H.; Jin, C.; Zhang, H.; Zhang, B. 15d-PGJ2 is a new hope for controlling tumor growth. *Am. J. Transl. Res.* **2018**, *10*, 648–658.
59. Fitzpatrick, F.A.; Wynalda, M.A. Albumin-catalyzed metabolism of prostaglandin D2. Identification of products formed in vitro. *J. Biol. Chem.* **1983**, *258*, 11713–11718. [[CrossRef](#)]
60. Maxey, K.M.; Hessler, E.; MacDonald, J.; Hitchingham, L. The nature and composition of 15-deoxy-Delta(12,14)PGJ(2). *Prostaglandins Other Lipid Mediat.* **2000**, *62*, 15–21. [[CrossRef](#)] [[PubMed](#)]
61. Parise, P.; Huybrechts, E.; Grasselli, S.; Falcinelli, F.; Nenci, G.G.; Gresele, P.; Vermylen, J. Generation of arachidonic acid metabolites from stimulated whole blood in patients with chronic myeloproliferative disorders. *Acta Haematol.* **1991**, *85*, 88–92. [[CrossRef](#)] [[PubMed](#)]
62. Tornhamre, S.; Stenke, L.; Granzelius, A.; Sjölander, M.; Näsman-Glaser, B.; Roos, C.; Widell, S.; Lindgren, J.A. Inverse relationship between myeloid maturation and leukotriene C4 synthase expression in normal and leukemic myelopoiesis-consistent overexpression of the enzyme in myeloid cells from patients with chronic myeloid leukemia. *Exp. Hematol.* **2003**, *31*, 122–130. [[CrossRef](#)]
63. Sjölander, M.; Stenke, L.; Näsman-Glaser, B.; Widell, S.; Doucet, J.; Jakobsson, P.J.; Lindgren, J.A. Aberrant expression of active leukotriene C(4) synthase in CD16(+) neutrophils from patients with chronic myeloid leukemia. *Blood* **2000**, *95*, 1456–1464. [[CrossRef](#)]
64. Roos, C.; Sjölander, M.; Stenke, L.; Tornhamre, S. Abnormal LTC4 synthase RNA degradation in neutrophils from CML patients. *Br. J. Haematol.* **2004**, *124*, 739–745. [[CrossRef](#)] [[PubMed](#)]
65. Zovko, A.; Yektaei-Karin, E.; Salamon, D.; Nilsson, A.; Wallvik, J.; Stenke, L. Montelukast, a cysteinyl leukotriene receptor antagonist, inhibits the growth of chronic myeloid leukemia cells through apoptosis. *Oncol. Rep.* **2018**, *40*, 902–908. [[CrossRef](#)]
66. Yektaei-Kari, E.; Zovko, A.; Nilsson, A.; Näsman-Glaser, B.; Kanter, L.; Rådmark, O.; Wallvik, J.; Ekblom, M.; Dolinska, M.; Qian, H.; et al. Modulation of leukotriene signaling inhibiting cell growth in chronic myeloid leukemia. *Leuk. Lymphoma* **2017**, *58*, 1903–1913. [[CrossRef](#)]
67. Sveinbjörnsson, B.; Rasmuson, A.; Baryawno, N.; Wan, M.; Pettersen, I.; Ponthan, F.; Orrego, A.; Haeggström, J.Z.; Johnsen, J.I.; Kogner, P. Expression of enzymes and receptors of the leukotriene pathway in human neuroblastoma promotes tumor survival and provides a target for therapy. *FASEB J.* **2008**, *22*, 3525–3536. [[CrossRef](#)]

68. Dahinden, C.A.; Clancy, R.M.; Gross, M.; Chiller, J.M.; Hugli, T.E. Leukotriene C4 production by murine mast cells: Evidence of a role for extracellular leukotriene A4. *Proc. Natl. Acad. Sci. USA* **1985**, *82*, 6632–6636. [[CrossRef](#)]
69. Pinto-Fernandez, A.; Salio, M.; Partridge, T.; Chen, J.; Vere, G.; Greenwood, H.; Olie, C.S.; Damianou, A.; Scott, H.C.; Pegg, H.J.; et al. Deletion of the deISGylating enzyme USP18 enhances tumour cell antigenicity and radiosensitivity. *Br. J. Cancer* **2021**, *124*, 817–830. [[CrossRef](#)] [[PubMed](#)]

Disclaimer/Publisher’s Note: The statements, opinions and data contained in all publications are solely those of the individual author(s) and contributor(s) and not of MDPI and/or the editor(s). MDPI and/or the editor(s) disclaim responsibility for any injury to people or property resulting from any ideas, methods, instructions or products referred to in the content.